Coupled effects of corrosion damage and sustained loading on the flexural behavior of RC beams strengthened with CFRP anchorage system

Pan, Tanbo; Zheng, Yonglai; Zhou, Yujue; Liu, Yongcheng; Yu, Kunlong; Zhou, Yubao

DOI
10.1016/j.compstruct.2022.115416

Publication date
2022

Document Version
Final published version

Published in
Composite Structures

Citation (APA)
Pan, T., Zheng, Y., Zhou, Y., Liu, Y., Yu, K., & Zhou, Y. (2022). Coupled effects of corrosion damage and sustained loading on the flexural behavior of RC beams strengthened with CFRP anchorage system. *Composite Structures*, *289*, Article 115416. https://doi.org/10.1016/j.compstruct.2022.115416

Composite Structures 289 (2022) 115416

Contents lists available at ScienceDirect

Composite Structures

journal homepage: www.elsevier.com/locate/compstruct

Coupled effects of corrosion damage and sustained loading on the flexural behavior of RC beams strengthened with CFRP anchorage system

Tanbo Pan [a], Yonglai Zheng [a], Yujue Zhou [a,b,*], Yongcheng Liu [a], Kunlong Yu [a], Yubao Zhou [c]

[a] Department of Hydraulic Engineering, Civil Engineering College, Tongji University, Shanghai 200092, PR China
[b] Department of Civil Engineering, Sanming University, Sanming 365004, PR China
[c] Faculty of Civil Engineering and Geosciences, Delft University of Technology, Delft 2600AA, Netherlands

ARTICLE INFO

Keywords:
CFRP anchorage system
Corrosion
Flexural behavior
Reinforced concrete
Strengthening
Sustained loading

ABSTRACT

This paper presents the results of an experimental study on the flexural behavior of carbon fibre reinforced polymer (CFRP) anchorage system strengthened reinforced concrete (RC) beams under the coupled effects of corrosion damage and sustained loading. The test beams were subjected to combined accelerated corrosion in 5% NaCl solution and sustained loads for 25, 50 and 100 days at 0% and 50% load levels of the virgin beam ultimate load capacity. The failure modes, load carrying capacity, deflection, ductility and strain response of the beams were investigated in detail. The results indicated that CFRP anchorage systems enhanced the yield and ultimate load of the corrosion-damaged beams. The use of CFRP anchorage system restored the ultimate load of corroded beams between 87.6% and 104.8% and the yield load between 81.9% and 92.7% with respect to those of the virgin beam. In contrast, the ductility and energy absorption index suffered a decline. CFRP-strengthened beams showed a reduction of 4.5%–28.9% for the ductility index compared with their counterparts without CFRP anchorage system. Sustained loads resulted in more considerable reductions in load-bearing capacity, greater loss of rebars mass, wider width of corrosion cracks, indicating a significant coupling effect between sustained loading and corrosion damage. Three typical failure modes of the CFRP-strengthened beams were observed and explained in the paper, thus revealing the failure mechanism of CFRP-strengthened beams. In the engineering practice of CFRP anchorage system, the coupled effects of corrosion damage and sustained loading on the strengthened systems should be taken into accountant comprehensively.

1. Introduction

Corrosion of steel reinforcement in concrete has recently emerged as a significant durability problem, especially in coastal environments prone to chloride erosion. Corrosion leads to structural degradation, such as loss of cross-sectional area of the bars, bond deterioration, concrete cracking, and concrete cover spalling [1–5]. Deteriorating RC structures caused by reinforcement corrosion not only result in a significant economic loss but also pose a significant hazard to engineering structures, which also gravely jeopardized human life safety [6,7]. Consequently, it is essential for most existing structures to repair and strengthen insufficient RC members.

Externally bonded FRP plates or sheets has been an extensively adopted technique in improving the durability and strength of reinforced concrete (RC) structures [8–11], given its lightweight and high tensile, excellent corrosion resistance, good stability, convenient construction, as well as minimal impact on structural appearance [12–14]. However, this method also has its inherent disadvantages. For instance, it has generally been found that premature debonding of the FRP from the concrete surface usually occurs at much lower strain levels than the FRP's ultimate strain [15,16]. To delay or prevent premature deboning of the FRP plates, three general anchorage techniques have been developed to date, namely mechanically fastened metallic anchors, U-jacket anchors and FRP anchors [17]. In engineering practice, the first two anchoring methods have shown problems such as inconvenience in construction and weak durability [18]. Hence, FRP anchors have gained increasing attention due to their high efficiency, ease of installation, and compact size. This method significantly improves the efficiency of FRP utilization.

Furthermore, numerous studies have documented the usage of FRP anchors to prevent premature debonding of FRP and heighten the performance of RC members. Kalfat et al. [19] have provided a detailed

* Corresponding aurthor.
E-mail address: 1710202@tongji.edu.cn (Y. Zhou).

https://doi.org/10.1016/j.compstruct.2022.115416
Received 14 October 2021; Received in revised form 23 December 2021; Accepted 21 February 2022
Available online 7 March 2022

Table 1
Test matrix.

Group	Specimens	Corrosion damage levels	Periods of accelerating corrosion process (days)	Sustained load levels (P/P_u)
–	UU	0	0	0
A	CU-5-HL	5%	25	50%
	CS-5-NL	5%	25	0
	CS-5-HL	5%	25	50%
B	CU-10-HL	10%	50	50%
	CS-10-NL	10%	50	0
	CS-10-HL	10%	50	50%
C	CU-20-HL	20%	100	50%
	CS-20-NL	20%	100	0
	CS-20-HL	20%	100	50%

review regarding FRP anchors applied to FRP-strengthened RC flexural members. ED Castillo et al. [20] examined the effect of five critical variables on the effectiveness of FRP anchors. They found that narrow-anchored FRP strips generated more fracture stresses than wide-anchored FRP strips and needed smaller anchor material ratios to be fully developed. Zheng et al. [21] provided experimental results of the residual bearing capacity and fatigue behavior of FRP-strengthened RC beams that have been anchored with FRP anchors. Experimental results showed that with increasing anchoring length, the performance of beams under monotonic and cyclic loads improves initially and later deteriorates. Kim et al. [22], Koutas et al. [23], Zaki et al. [24] adopted FRP anchors to avoid the premature debonding of RC beams with FRP. Each of these studies indicated a considerable increase in flexural or shear capacity as a result of the adoption of FRP anchors. This rise grows as the quantity and fiber of the FRP anchor contents increase to reach the full sectional capacity. Moreover, the closer the distance between the anchors also results in higher flexural ability.

Nonetheless, little attention has been paid to the feasibility of using FRP anchorage systems to strengthen corroded concrete members. The research on corroded reinforced concrete members faces a dual challenge; namely, the simulation of natural corrosion conditions and the durability of the repair system should include corrosion recovery. Considering the prevalence of corrosion of reinforcement in marine structures in service under loading, the simulation of the natural marine environment should take into account both factors (including sustained loading and corrosion) as much as possible. To date, there are only a few studies on the coupling effect of corrosion damage and sustained loading on the performance of FRP-reinforced RC members. El Maaddawy et al. [25] investigated the effect of sustained loading on the flexural behavior of CFRP-reinforced RC beams exposed to a corrosive environment. The results showed that the presence of sustained loading increased the mass loss rate and decreased the yield load of the reinforced concrete beams, but had no significant effect on the ultimate strength of the reinforced concrete beams. In another study, Zhou et al. [26] tested the bond behavior of corroded rebars under FRP confinement and sustained loads. It revealed that the dual action of FRP lateral restraint and sustained loads decreased the influence of the corrosion rate and dramatically improved the interfacial bond performance and ductility.

In summary, there is still a lack of knowledge on the performance of corroded RC members strengthened by the FRP anchorage system. In this study, an experimental investigation was conducted on the flexural behavior of corroded RC beams strengthened by the CFRP anchorage system at three different levels of corrosion damage (i.e., 5%, 10%, 20%). To simulate the natural behavior of in-service RC structures, the tested beams were exposed to the environment of accelerated corrosion, which was applied to the sustained loads by a monotonic four-point loading. The failure modes, loading bearing capacity, ductility, the development of cracks, and the strain action of CFRP were recorded and analyzed, and the coupling effects of corrosion damage and sustained loading were investigated.

2. Experimental program

2.1. Test matrix

Table 1 summarizes the test matrix. The test parameters included the periods of accelerated corrosion and sustained loading levels. One beam that was not corroded or strengthened was used as a control. The remaining beams were divided into three groups and subjected to accelerated corrosion for 25, 50, and 100 days, respectively. In each group of the corroded specimens, two specimens were simultaneously subjected to accelerated corrosion and sustained load (50% of the ultimate loading capacity of the virgin beam), while the remaining one was only exposed to accelerated corrosion without sustained load. At the end of the corrosion process, one beam without a sustained load in each group was not strengthened and was used as a benchmark, while other beams were strengthened with the CFRP anchorage systems.

The beams were labeled following the form of X-Y-Z. 'X' indicates the state of the beams. UU, CU, CS denotes Uncorroded-Unstrengthened, Corroded-Unstrengthened, Corroded-Unstrengthened, respectively. 'Y' represents the corrosion damage level, 'Z' stands for the sustained loading level.

2.2. Test specimen and materials

The geometry and reinforcement details of concrete beams are shown in Fig. 1. All beams were 1600 mm long, with cross-sectional width b = 150 mm and height h = 200 mm. the concrete protective layer thickness was 25 mm. All beams were reinforced with 2–14 M (14 mm diameter) deformed reinforcement at the bottom and 2–8 M (8 mm diameter) deformed reinforcement at the top. The test beams were designed to sustain bending damage under four-point bending loads. To avoid shear damage, the shear span was reinforced with 6 M (6 mm

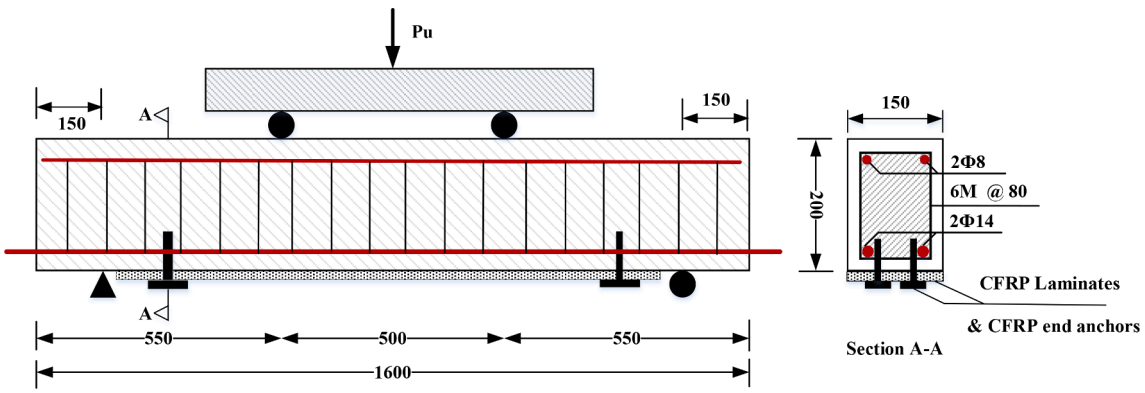

Fig. 1. The geometry and reinforcement details of concrete beams (dimensions in millimetre).

Table 2
Material properties.

Materials	Strength and strain		Elastic modulus
Concrete	Compressive strength	42.5 ±3.6 MPa	-
D14	Yield strength	615.7 ±16.2 MPa	200 GPa
	Ultimate strength	462.2 ±5.5 MPa	
D8	Yield strength	611.3 ± 15.2 MPa	200 GPa
	Ultimate strength	408.9±4.5 MPa	
CFRP sheet	Tensile strength	3000 MPa	230 GPa
	Ultimate tensile strain	1.66%	

diameter) deformed hoops with a hoop spacing of 80 mm. Epoxy resin was applied to the contact position between the stirrup and the tensile reinforcement to prevent corrosion of the stirrups.

The properties of the material are summarized in Table 2. All beams were cast with an ordinary weight concrete mixture having equivalent compressive strength. Six standard concrete columns (150 × 300 mm) were prepared with ordinary concrete. The compressive strength of the concrete cylinders was 42.5 MPa with a standard deviation of 3.6 MPa. The yield strengths of the longitudinal reinforcement for 14 M and 8 M were 462.2 MPa (with a standard deviation of 15.2 MPa) and 408.9 MPa (with a standard deviation of 5.5 MPa), respectively. The ultimate strengths of the longitudinal reinforcement for 14 M and 8 M were 615.7 MPa (with a standard deviation of 16.2 MPa) and 611.3 MPa (with a standard deviation of 4.5 MPa). The material properties of the CFRP sheet were provided by the manufacturer, including layer thickness of 1.02 mm, tensile strength of 3000 MPa, ultimate tensile strain of 1.66%, and tensile modulus of 230 GPa.

2.3. Test of accelerated corrosion combined with sustained loading

In order to ascertain the sustained load of the tested beams, beam UU was subjected to monotonic four-point-bending loading to obtain ultimate loading capacity. The method for coupling corrosion and sustained loading was as follows:

(1) Moved RC beams into the loading device, then applied the sustained load to the predetermined level by mechanical jack and transmitted to the strengthened beams through a distribution beam. A pressure transducer measured the magnitude of the sustained load. (as illustrated in Fig. 2)
(2) A customized water tank was set up at the bottom of the cross-beam and filled with 5% NaCl solution as the corrosion medium. After seven days of immersion, a stainless steel mesh was positioned at the near-surface of the underwater segment. The tensile longitudinal reinforcements of the beam were connected to the positive pole of the power supply as the anode and the stainless-steel mesh was connected to the negative pole of the power

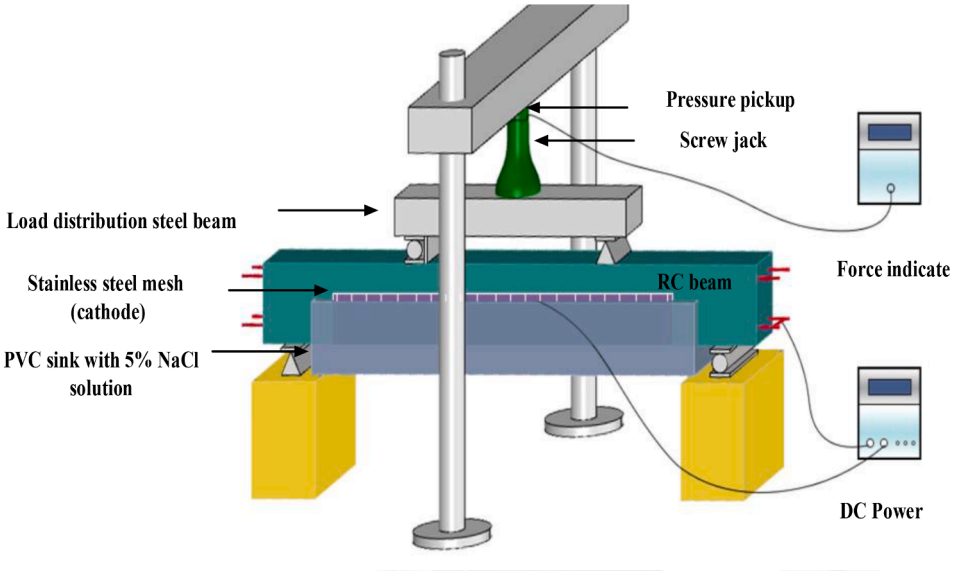

Fig. 2. Test set-up for coupling corrosion and sustained loading.

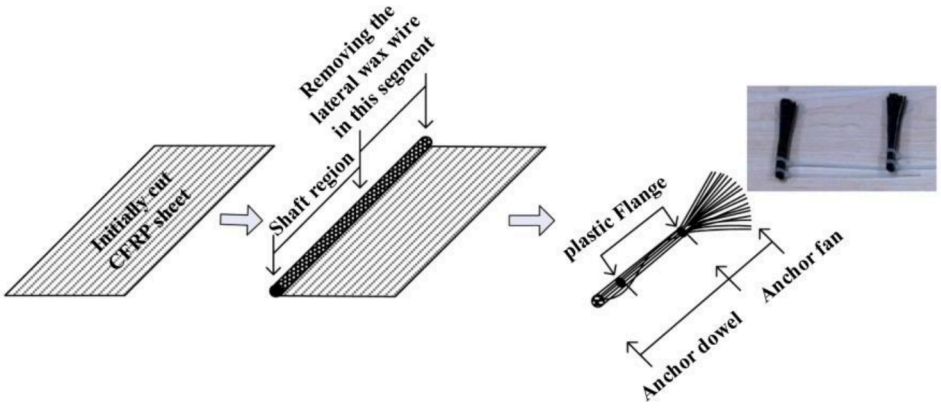

Fig. 3. Construction of CFRP anchors.

(a) Concrete drilling (b) CFRP anchors inserted into concrete (c) Bonding of the CFRP sheet and anchors with epoxy resin

Fig. 4. Anchors installation procedure.

Fig. 5. Monotonic four-point loading of CFRP-strengthened RC beams.

supply as the cathode [27]. It is worth noting that the negative pole of the power supply is connected to the wire mesh wrapped at the middle of the span so as to ensure the uniformity of the corrosion effect.

To simulate natural corrosion and avoid the bond loss at the interface between concrete and steel, the ampere density should be less than 200 $\mu A/cm^2$ [28]. Therefore, the test was performed using a constant electrical current of 205 mA with an ampere density of 180 $\mu A/cm^2$. The theoretical mass loss of tensile reinforcement can be calculated by Faraday's second law [Eq. (1)] so as to obtain three kinds of tested beams with different degrees of corrosion.

$$\text{Mass loss} = \frac{ItM}{Fn} \tag{1}$$

where I = constant current (A), t = corrosion duration (s), M = the atomic weight of iron (equal to 55.847 *g/mol*), F = Faraday's constant (equal to 96,485*C/mol*), n = the ion charge.

As mentioned above, the period of accelerating the corrosion process combined with sustained loading was 25, 50, 100 days, respectively, for a mild, moderate, severe degree of corrosion damage (5%, 10%, 20%).

2.4. CFRP anchor systems

2.4.1. CFRP anchors construction

An in-depth explanation of the manufacturing process for the CFRP anchors is given by Smith and Zhang, as well as instructions on how to install the CFRP anchors and sheets [29,30]. The manufacturing method of CFRP anchors in this research is described below. As shown in Fig. 3, each CFRP anchor was constructed using a 150 mm wide by 80 mm long rolled unidirectional CFRP sheet. The 80 mm length is formed by a 50 mm long fan and a 30 mm pre-built section, which includes a small margin for a 90-degree bend section. According to Llauradó [31], the hardened length should not exceed two-thirds of the embedment length to prevent damaging the bending area; hence, epoxy was applied to an end part spanning ten millimeters over the whole width of the sheet to produce the hardened shaft. The nominal diameter of the dowel in bow-tie CFRP anchors produced from 150 mm broad CFRP sheets was 10 mm. The detailed construction process is available in our previous study [21].

2.4.2. Anchors installation

The primary strengthening steps for tested beams are depicted as follow:

(1) Four holes with diameters of 10 mm diameter and depths of 35 mm were drilled into the bottom faces of the beams (as shown in Fig. 4a). To ensure a better adherence between the concrete surface and epoxy resin, pressurized air and a vacuum was used to remove concrete particles and dust from the drilled holes and the bottom surface of the beams.
(2) Then, the surface of the concrete to be reinforced was prepared with a pneumatic needle scaler. This surface preparation removed the top surface of the weakened concrete, exposing the aggregates across the area where the CFRP sheets were to be bonded and also roughening the concrete surface [32].
(3) Each drilled hole was then half-filled with epoxy resin, and a layer of CFRP sheet with a length of 1300 mm and a width of 150

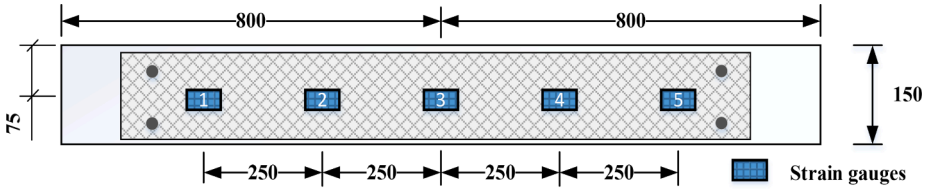

Fig. 6. The lay-out of strain gauges along with the CFRP sheet (dimensions in millimetre).

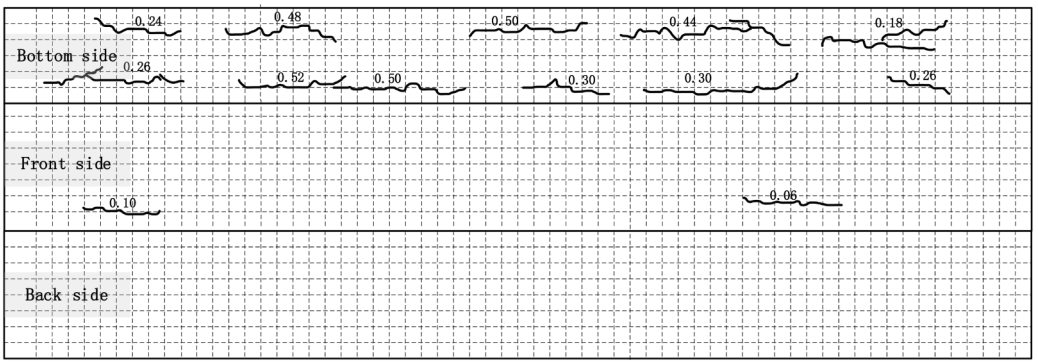

(a) CS-5-NL

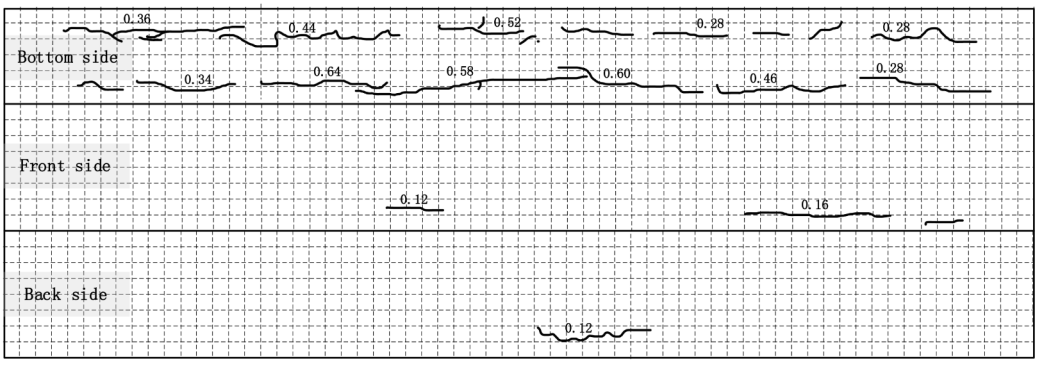

(b) CS-5-HL

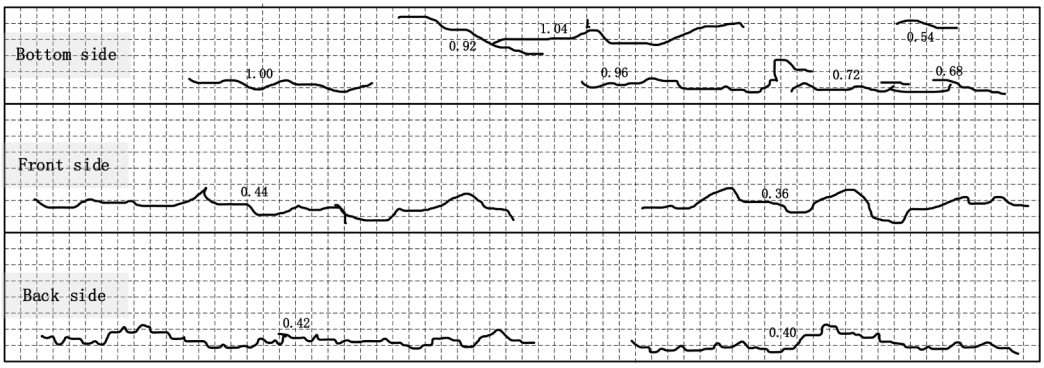

(c) CS-10-NL

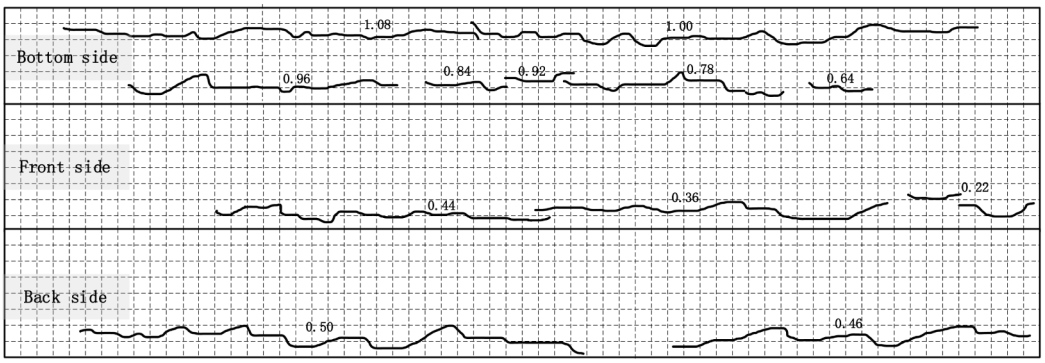

(d) CS-10-HL

Fig. 7. Corrosion cracks patterns.

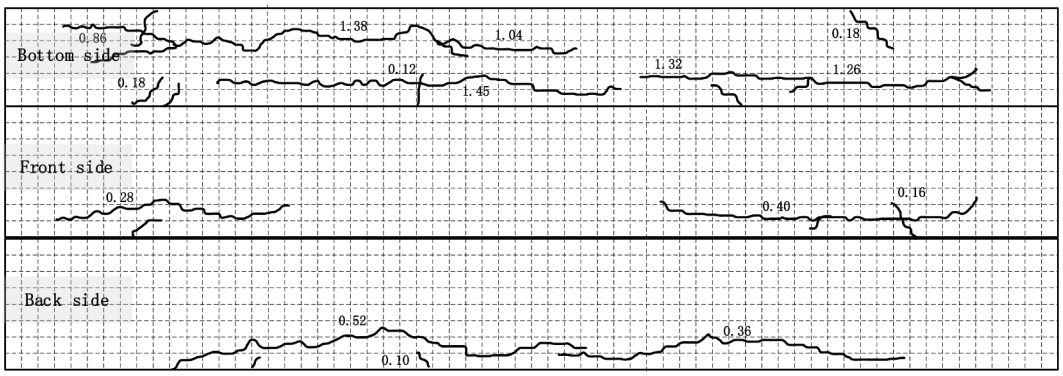

(e) CS-20-NL

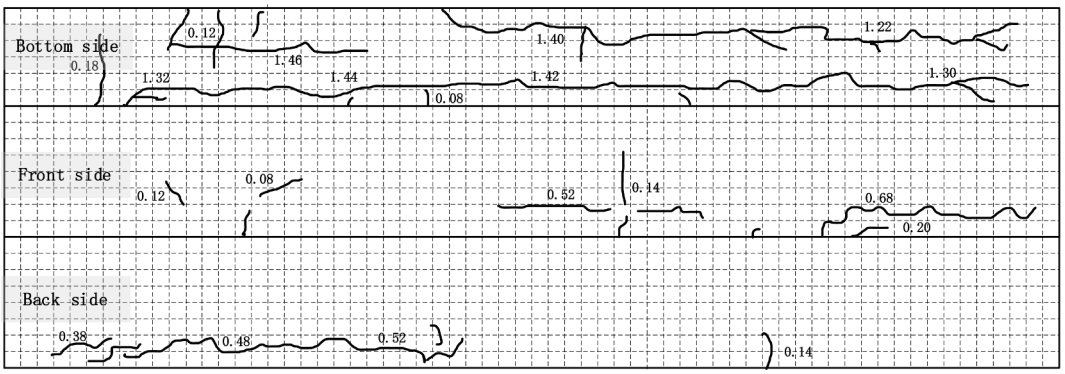

(f) CS-20-HL

Fig. 7. (*continued*).

Table 3
Summary of the test results.

Beams	$w_{avg}(mm)$	W_{grave}(%)	P_y(kN)	P_u(kN)	P_{yNor}[a](kN)	P_{uNor}[a](kN)	Mode of failure
Virgin beam							
UU	–	–	113	125.34	1	1	CC
Group A: Theoretical mass loss of 5%							
CU-5-HL	0.60	5.2	101	119.3	0.929	0.952	CC
CS-5-NL	0.5	4.7	107	136	0.947	1.085	CD-AP(CB)
CS-5-HL	0.64	5.3	104.8	131.4	0.927	1.048	CSS
Group B: Theoretical mass loss of 10%							
CU-10-HL	1.05	10.3	98	111.3	0.867	0.888	CC
CS-10-NL	1.00	8.9	99	126.8	0.876	1.012	CD-AP(CB)
CS-10-HL	1.08	10.5	92.6	121.2	0.819	0.967	CD-AP(BF)
Group C: Theoretical mass loss of 20%							
CU-20-HL	1.44	19.6	83.49	102.6	0.739	0.819	CC
CS-20-NL	1.45	18.7	95.8	115	0.848	0.925	CD-AP(BF)
CS-20-HL	1.46	19.3	97	109.8	0.858	0.876	MC-FR

[a]Normalised with respect to the virgin beam.

mm was externally bonded onto the strengthened area using the wet lay-up technique.

(4) The CFRP anchors were inserted into the holes after passing through the CFRP sheet (as shown in Fig. 4b). It is worth noting that the insertion of CFRP anchors should avoid cutting off the fibre. Next, more epoxy resin was applied to fill the holes until the surface was parallel to the CFRP sheets, and the free ends of the CFRP anchors were unfolded outward and bonded to the surface of the CFRP sheet with epoxy resin to form a complete CFRP anchorage system. The process of CFRP anchorage system installation is shown in Fig. 4.

2.5. Test set-up and instrumentation

To obtain the residual strength of laboratory beams, monotonic four-point loading tests were performed on all beams, as shown in Fig. 5. All tests were conducted with the MTS drive at a speed of 1 mm/min for displacement control. The deflections at the mid-span and two loading points of the beams were monitored by linear variable displacement transducers (LVDTs). One strain gauge was placed at the top of the test beam in the mid-span pressure zone. Five strain gauges were distributed evenly throughout the fiber of the CFRP-reinforced beam, as shown in Fig. 6.

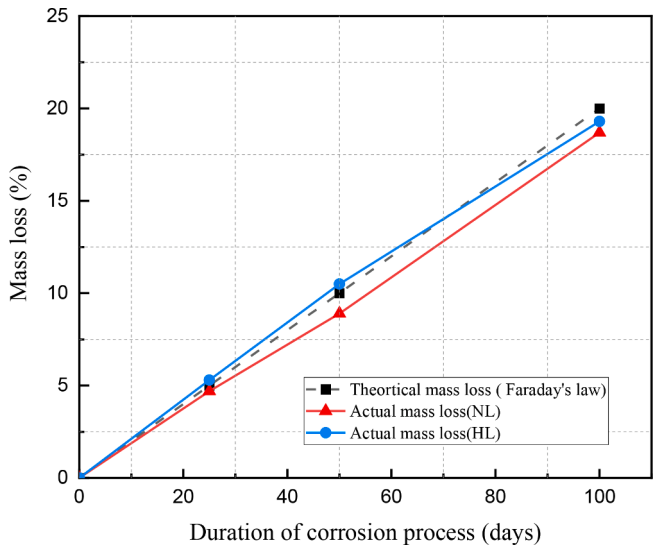

Fig. 8. Theoretical and actual mass loss versus the duration of the corrosion process.

3. Experimental results and discussion

3.1. Corrosion behavior

3.1.1. Corrosion observations

The concrete cover started to crack with the accumulation of damage induced by corrosion. After each beam reached its corrosion time, the RC beams were removed from the reaction tank and the reddish-brown corrosion products at the cracks on the concrete surface were washed out. In order to evaporate the moisture on the concrete surface, the tested beams needed to be placed in a natural environment for 12 h. All cracks on the bottom and sides of each beam were depicted on square grid paper following the crack direction, and the maximum width of each crack was measured using a crack gauge, with each grid corresponding to a 50 mm × 50 mm area of the realistic beam. It was observed that the overall trend of longitudinal cracks was along the direction of the longitudinal tensioned reinforcement at the bottom of the beam. The length of the cracks in the pure bending zone at the bottom of the beam was the longest, and the width of the cracks was greater, and the widest part of the cracks was generally near the span position of the beam. The corrosion cracks patterns are shown in Fig. 7.

Table 3 lists the maximum corrosion crack width, w_{max}, for each beam. The values of the maximum crack width were 0.64, 1.08, and 1.42 mm for groups A, B, and C, respectively; hence, the crack width increased proportionally as the corrosion duration increased. Besides, it can be obviously observed that the crack width of beams exposed to the sustained loading was larger than that of beams without the sustained loading with the same corrosion duration. For instance, at low levels of corrosion, the corrosion crack width was 0.64 mm for beam CS-5-HL, an increase of 22.2% compared to beam CS-5-NL (Fig. 7a, b). At a severe level of corrosion, however, the corrosion crack width was 1.46 mm for beam CS-20-HL, almost the same as beam CS-20-NL (Fig. 7e, f). This implied that in the early phases of corrosion, the sustained loading causes the cracks to grow faster, thereby speeding the corrosion further, expanding the fractures; however, when it reaches a high degree of corrosion, sustained loading has only a partial effect on corrosion crack width.

3.1.2. Mass loss of reinforcements

After testing the corroded beams, the tensile longitudinal bars were carefully removed to calculate each beam's actual steel mass loss. Specifically, three steel coupons, each 200 mm long, were taken from each corroded tensile reinforcement. The collected rebar coupons were then cleaned, dried, and weighted according to the guidelines of the ASMT G1-03 standard [33]. The actual steel mass loss of each beam was determined as the average mass loss of the three steel coupons.

Table 3 lists the actual steel mass for each corroded beam. For beams without sustained loading, the average gravimetric mass loss of corroded beams was measured equal to 4.7%, 8.9%, and 18.7%, respectively, corresponding to theoretical mass losses of 5, 10, and 20% predicted from Eq. (1). On the other hand, their counterparts exposed to sustained loading had an average mass loss of 5.2% (beam CS-5-HL), 10.3% (beam CS-10-HL), and 19.3% (beam CS-20-HL), respectively. It is worth noting that corroded beams with sustained loading exhibited a higher corrosion level than corroded beams in normal conditions. The discrepancy between the theoretical and actual mass losses in the steel bars is shown in Fig. 8. This discrepancy was attributed to the external load action leading to the microcracks growth, which allows more chloride ions and oxygen to enter the beam and spread to the surface of the reinforcement, thereby accelerating the process of corrosion of the reinforcement [34].

3.2. Flexural behavior after corrosion

3.2.1. Failure modes

The failure modes of all nine test beams are summarized in Table2. Photographs of typical failure mechanisms are shown in Fig. 9. The beam UU (control) and the CU (corroded unstrengthened) have similarities in crack patterns and failure modes. They failed by yielding tensile bars followed by the crushing of top concrete (referred to as "CC" for simplicity in Table 3). Large transversal cracks occurred at the constant moment zone as the load exceeded the cracking load. (see Fig. 9a). On the other hand, the failure modes of corroded beams strengthened with the CFRP anchorage system were diverse. The failure modes were affected by several factors, including the parameters of the CFRP anchor system and the corrosion-damaged degree of steel bars. To achieve a better understanding of the failure mechanism of CFRP-strengthened beams and the combined effects of accelerated corrosion and sustained loading, all distinct failure modes are explained in detail as follows.

1 Concrete cover separation

This type of failure was reported for beam CS-5-NL, as shown in Fig. 9b. In this mode, it can observe that the concrete cover at the bottom was coming off extensively (referred to as CCS). It is worth noting that there was no debonding at the interface between the CFRP sheet and the concrete. This failure mode was more brittle than that of other strengthened beams, probably due to the fact that the corrosion cracks and flexural cracks being interlinked, causing the concrete to fall off at the bottom.

2 Debonding of CFRP sheet followed by pulling out of anchors

This type of failure occurred at the CFRP/matrix interface with debonding between the CFRP sheet and the concrete substrate near the end of the sheet, followed by anchors pull-out nearby (referred to as CD-AP), as shown in Fig. 9c, d. The debonding was caused by the propagation of flexural cracks to this thin layer of the matrix and the relative deformation between the fabric and the matrix. Debonding was caused by the extension of bending cracks into the thin layer of the substrate and the relative deformation between the fabric and the substrate. This damage pattern was observed in CS-5-HL, CS-10-NL, CS-10-HL and CS-20-NL beams. In terms of CFRP anchors, two main failure modes were observed in this study: a combination of pull-out and concrete cone failure (CB), CFRP-to-epoxy bond failure (BF), as shown in Fig. 9c, d. It should be noted that the addition of anchors retarded the debonding of the carbon fiber fabric and the damage mode shifted to progressive

(a) CC in Beam UU

(b) CSS in Beam CS-5-NL

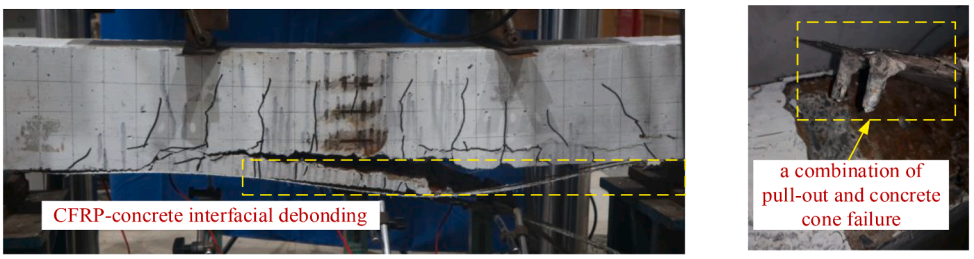

(c) CD-AP(CB) in Beam CS-5-HL

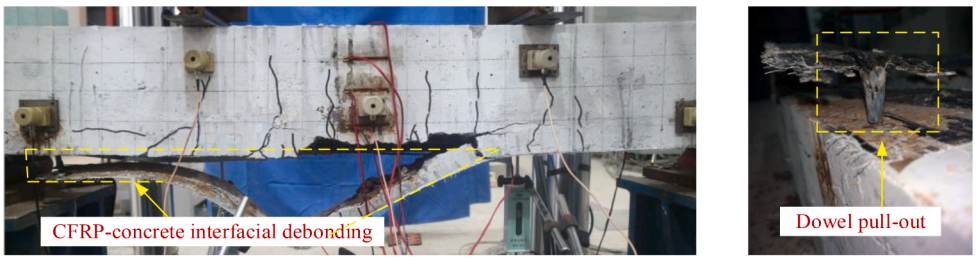

(d) CD-AP(BF) in Beam CS-10-HL

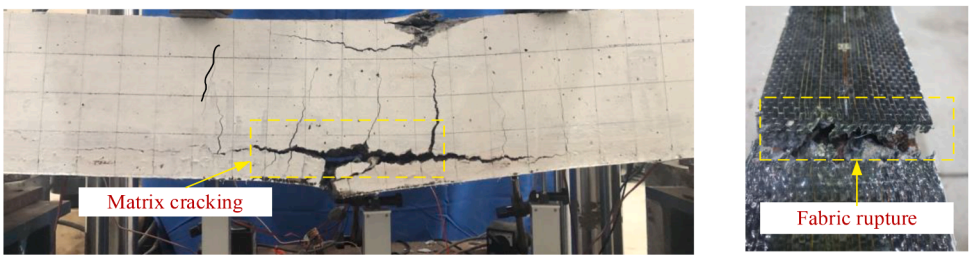

(e) MC-FR in Beam CS-20-HL

Fig. 9. Modes of failure.

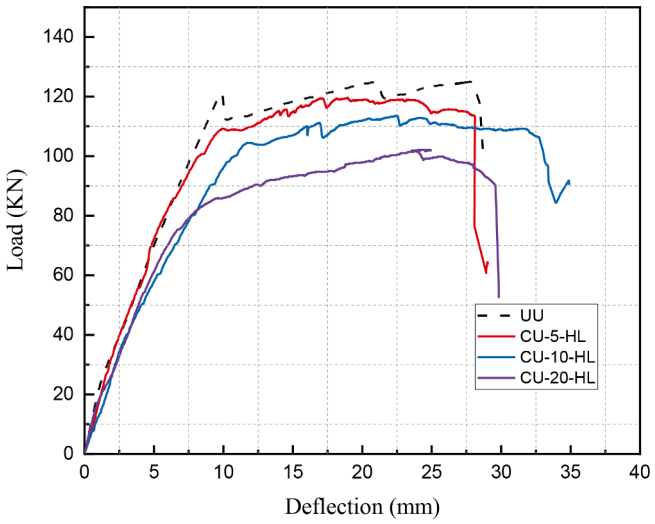

Fig. 10. Load-deflection curves for corroded-unstrengthened beams.

debonding of the fabric. As a result, this type of beam exhibited greater ductility compared to the specimens that failed due to anchor pull-out and concrete cover separation.

3 Matrix cracking and fabric rupture (MC-FR)

As shown in Fig. 9e, this type of failure occurred in the beam with a high degree of corrosion, i.e. CS-20-HL. With increasing load, the concrete matrix at the span of the sheet/concrete interface started to crack progressively, followed by fracture of the CFRP sheet. Neither interfacial debonding nor anchors pull-out was observed during the loading process. Instead, the CFRP sheet ruptured near the loading point. This failure of mode was mainly attributed to the stress concentrations in the span of the CFRP sheet caused by the cracked concrete.

3.2.2. *Load-Deflection response*

The mid-span deflection under monotonic four-point load was measured. The load–deflection relationships for the test beams are shown in Figs. 10-11. The flexural response of the strengthened beam is related to the duration of accelerated corrosion and the magnitude of the sustained loading.

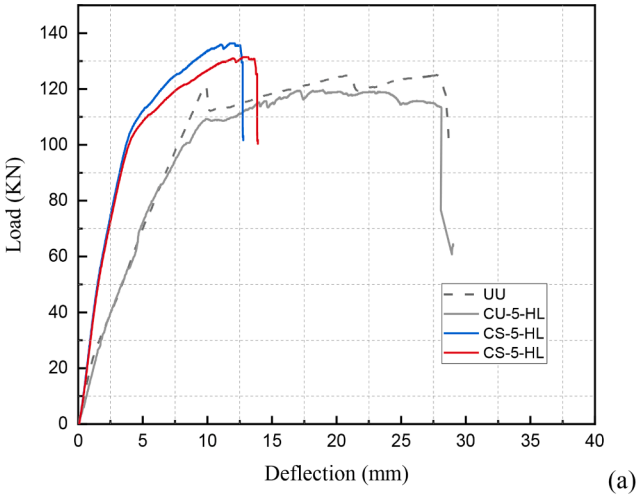

Beams of Group A

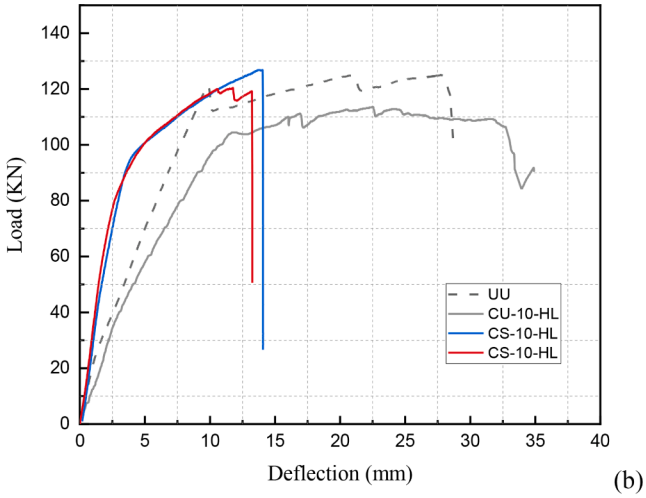

Beams of Group B

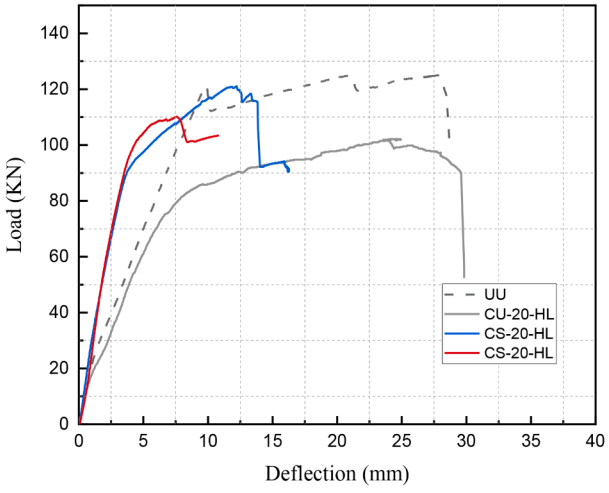

(c) Beams of Group C

Fig. 11. Load-deflection curves for beams with different corrosion degrees.

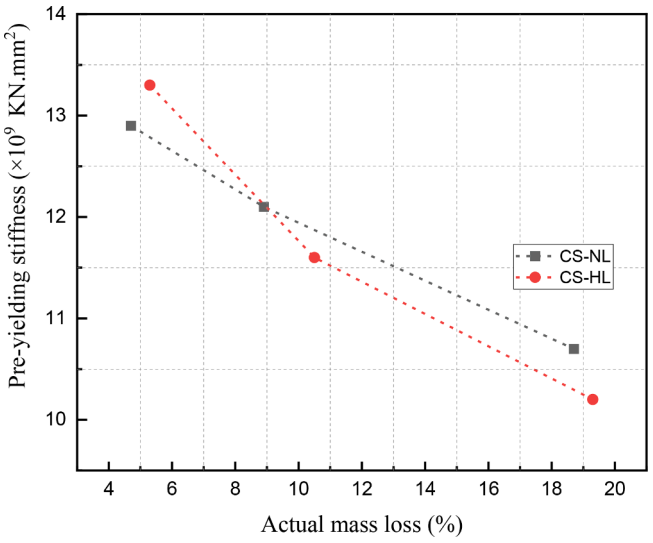

Fig. 12. Pre-yielding stiffness curves.

Fig. 10 shows the load–deflection curves of the virgin beam (UU) and the corroded unstrengthened beams (CU-5-HL, CU-10-HL, and CU-20-HL). All reinforced beams exhibited a similar flexural response. The load–deflection curves consisted of three phases with two turning points indicating tensile cracking of the concrete and yielding of the reinforcement. It was evident that there are multiple peaks in the curves, which is similar to that of comparable studies [35,36]. Furthermore, the load–deflection curve of unstrengthened beams indicated that corrosion slightly reduced the load-carrying capacity and stiffness of the beam.

Fig. 11 illustrates the load–deflection curves for the beams strengthened by the CFRP anchorage system. The load–deflection curves of the strengthened beams can be divided into two stages: before yielding and after yielding. In the initial stage of the whole loading process, i.e., the elastic stage, the loading value increased sharply; in the second stage, the deflection increased rapidly, and the load increased slightly due to the yielding of the steel reinforcement. All CFRP-reinforced beams had similar and significantly higher stiffness before yielding of the tensile reinforcement compared to unreinforced beams, indicating that the CFRP anchorage system was an important contributor to the development of pre-yield stiffness. This was attributed to the presence of CFRP sheets and anchors on the bottom of beams that delayed CFRP premature debonding from the concrete substrate and greatly heightened the flexural performance of beams.

Fig. 12 shows the relationship between the pre-yielding stiffness of the reinforced beams and the actual corrosion rate. As can be seen, the

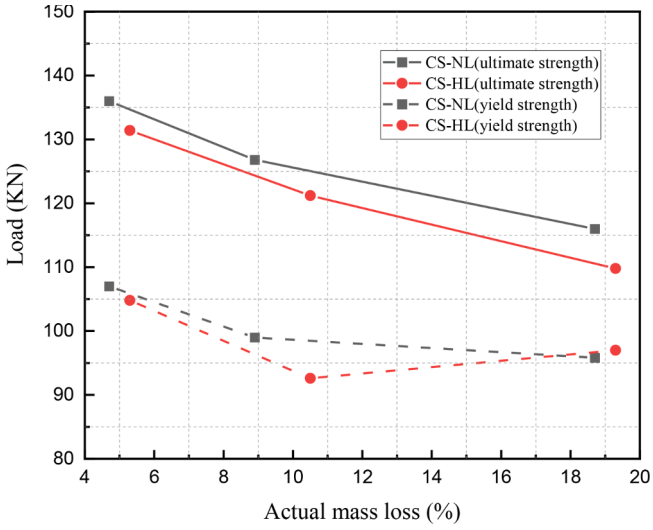

Fig. 14. Effect of sustained loading on the load capacity of strengthened beams.

Table 4
Ductility and energy absorption of the tested beams.

Beams	Mid-span displacement (mm)		Ductility index		Energy absorption index	
	δ_y(mm)	δ_u(mm)	ΔI	$\Delta I_{Nor}{}^a$	β	$\beta_{Nor}{}^a$
UU	9.07	28.50	3.14	1	3018.00	1
CU-5-HL	8.40	28.10	3.35	1.065	2926.78	0.969
CS-5-NL	4.10	12.71	3.10	0.987	1335.45	0.442
CS-5-HL	3.86	12.36	3.20	1.019	1429.39	0.474
CU-10-HL	8.76	32.70	3.73	1.188	2812.16	0.932
CS-10-NL	4.20	14.07	3.35	1.066	1266.56	0.420
CS-10-HL	3.82	13.25	3.47	1.104	1364.40	0.452
CU-20-HL	8.00	29.50	3.69	1.174	2353.82	0.780
CS-20-NL	4.66	13.86	2.97	0.947	1522.49	0.504
CS-20-HL	4.00	8.46	2.11	0.673	927.47	0.307

[a]Normalised with respect to the virgin beam.

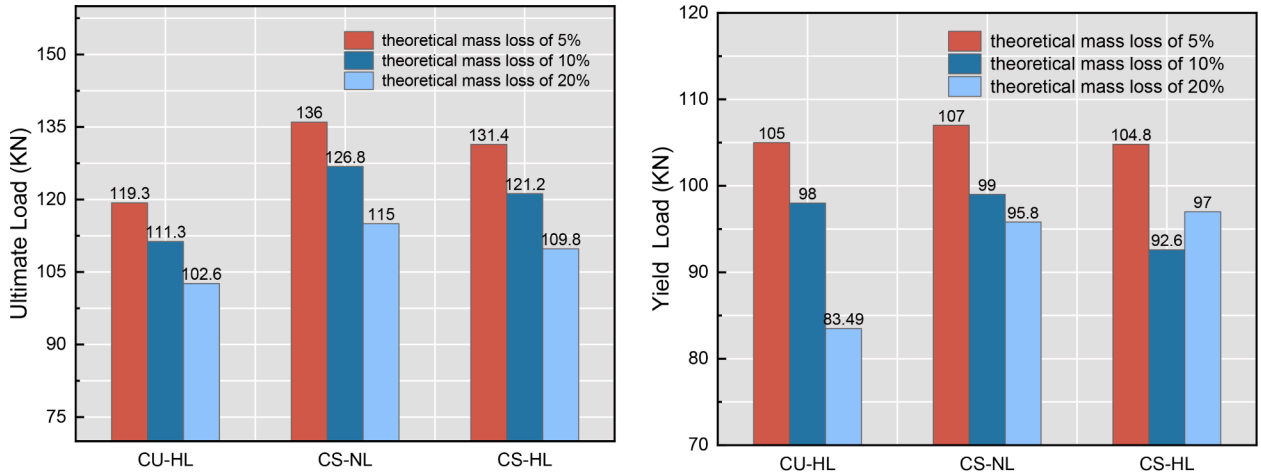

(a) Ultimate strength (b) Yield strength

Fig. 13. Effect of corrosion damage on the load capacity of strengthened beams.

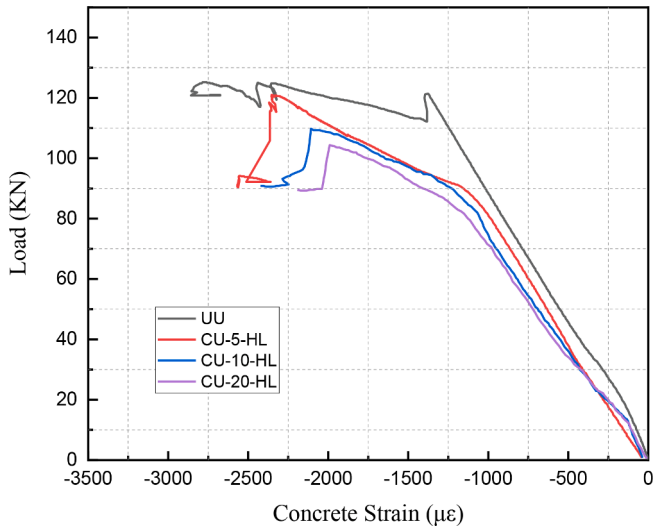

Fig. 15. Load-strain relationships for unstrengthened beams.

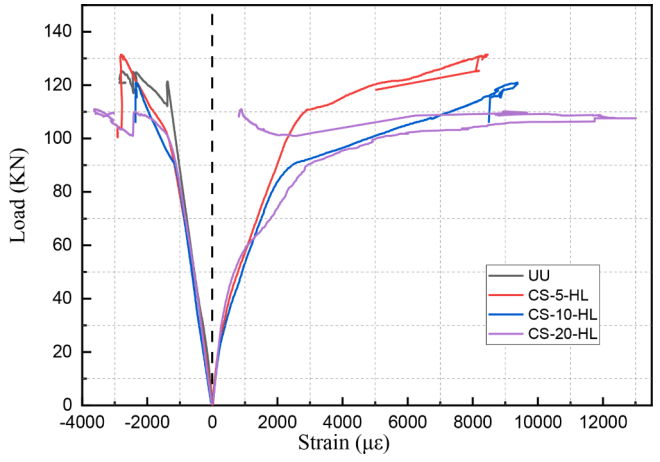

Fig. 16. Load-strain relationships for CFRP-strengthened beams.

stiffness of all reinforced beams decreased with increasing corrosion rate; also, the action of sustained loading showed a two-way response to the stiffness of the beam as the corrosion rate increased: first promoting and then inhibiting. Flexural cracks had developed in the tensile zone of the corroded beam during the sustained loading and extended along the beam body to the compression zone, which accelerated the corrosion process. At a low degree of corrosion damage, the expansion of corrosion products surrounding the tensile steel filled the flexural cracks and increased the compactness of concrete to improve the grip between concrete and steel; thereby, the sustained loading had a positive effect on the stiffness. At a high degree of corrosion damage, the accumulation of corrosion products led to severe concrete cracking, thus weakening the bond capacity between the reinforcement and the concrete, resulting in a reduction in the stiffness of the member. Hence, the sustained loading inhibited the stiffness of CFRP strengthened beams when the corrosion degree was higher. Further studies, which take these variables into account, will need to be undertaken.

3.2.3. Strength analysis

Table 3 summarizes the yield load, P_y, the ultimate load, P_u, of all beams. As shown in Fig. 13, the load capacity of corroded beams gradually decreased with an increasing corrosion ratio. The yield and ultimate loads of the unstrengthened beams (CU-5-HL, CU-10-HL, and CU-20-HL) were decreased by 3% and 4%, 7% and 8%, and 14% and 16%, respectively, in comparison to the virgin beam. Besides, the average mass loss of reinforcement was measured equal to $m_{grav} = 5.2\%$ for beam CU-5-HL, $m_{grav} = 10.3\%$ for beam CU-10-HL and $m_{grav} = 19.6\%$ for beam CU-20-HL. The reduction of loading-carrying capacities was less than the mass loss of steel. This is because the tensile bars lost their lugs from corrosion, resulting in a loss of mass without an equivalent loss of the effective cross-sectional area of the bars [37]. The corrosion deterioration of structural members evidently requires attention in order to ensure structural safety.

Fig. 13 shows the effect of corrosion degree on the load capacity of the reinforced beams. The use of CFRP anchor systems in beams CS-5-HL restored 92.7% and 104.8% of the yield and ultimate loads of the virgin beam, respectively. Increasing the corrosion level further decreased the yield and ultimate loads (beam CS-10-HL restored 81.9% and 96.7%, and beam CS-20-HL restored 85.8% and 87.6% of the yield and ultimate loads, respectively). Nevertheless, the change in strength was not linearly proportional to the degree of corrosion. Also, all the CFRP-strengthened beams exhibited a yield strength of 95.8 kN to 107 kN were well below the control, and the change was not significant. It was also attributed that the CFRP anchorage system significantly increased the stiffness of the corroded beam, which is mainly determined by the CFRP anchorage system.

Fig. 14 illustrates the influence of the sustained loading on the flexural strengths of the CFRP-strengthened RC beams. As shown in Fig. 14, the effect of corrosion on load capacity is correlated with the level of sustained loading. For group A (theoretical mass loss of 5%), beam CS-5-HL showed a decrease of 2.0% and 2.6% of the yield and ultimate strengths, respectively, in comparison to beam CS-5-NL. For Group B (theoretical mass loss of 10%), the yield and ultimate strength of CS-10-NL beams were 6.5% and 4.4% lower than those of CS-10-NL beams. For group C (theoretical mass loss of 20%), the ultimate strength of beam CS-20-HL decreased by 4.5%, while the yield strength increased by 1.3%. On the basis of these results, it can be concluded that the yield and ultimate load of the CFRP-strengthened beams with sustained loading are inferior to that of the beams without sustained loading, except for the yield capacity of beam CS-20-HL. This indicated that the accelerated corrosion process combined with sustained loading caused an adverse effect on the yielding and ultimate load of the CFRP-strengthened beams, especially in the cases of more significant corrosion damage.

3.2.4. Ductility and energy absorption

The deflection ductility index (ΔI) was calculated as the ratio of the mid-span deflection at the ultimate δ_u to the mid-span deflection at the yield δ_y. The energy absorption index β was defined as the area of the load–deflection curve from 0 to the ultimate point. The flexural ductility index and energy absorption index of the test beam are shown in Table 4.

As seen in Table 4, compared to the virgin beam (UU), the corrosion-damaged beams exhibited much better ductility performance. The unstrengthened beams (CU) showed the ductility index of 3.35, 3.73, and 3.69, respectively, 106.5%, 118.8%, and 117.4% of the virgin beam. It can be noticed that the ductility index,ΔI, would increase and then decrease as the increase corrosion level of beams. On the other hand, the virgin beam's energy absorption index (3018.00 J) was superior to those (2926.78 J, 2812.16 J, 2353.82 J) of the unstrengthened corroded beams by 3.1%, 6.8%, and 22.0%, respectively. This finding indicated that corrosion damage of steel bars is a significant contributor to the energy absorption index, and the degree to which it was reduced was correlated with the degree of corrosion damage for steel bars.

For the set of beams with the same theoretical mass loss, these strengthened beams showed a 4.5%–28.9% decrease in their average ductility indexes compared to their counterparts without the strengthened method. Beam CS-10-NL and beam CS-10-HL recorded ductility indexes of 3.35 and 3.47, respectively, and exhibited the most excellent ductility performance with respect to other strengthened beams.

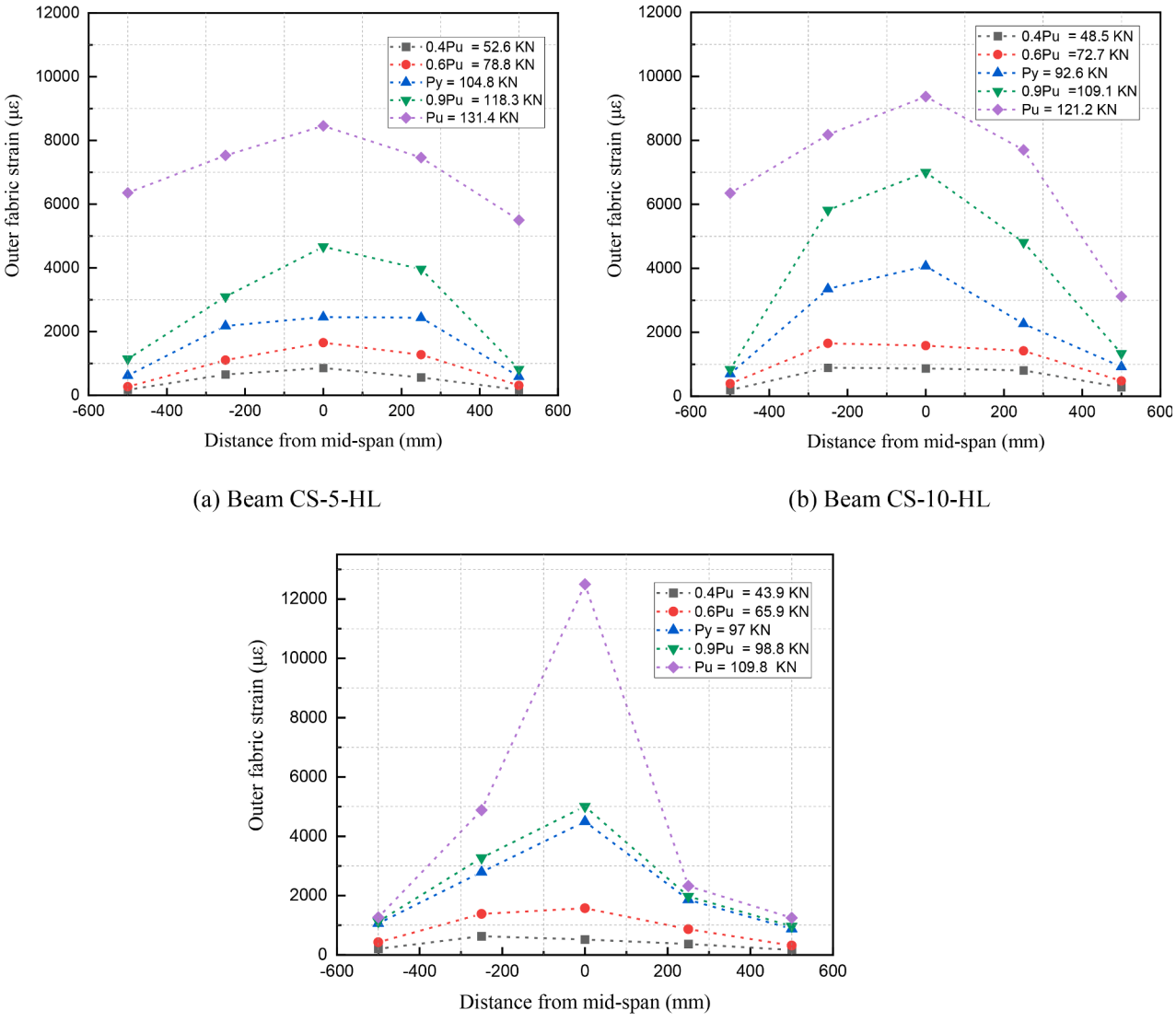

Fig. 17. The outer fabric tensile strain distributions on the CFRP sheet.

Additionally, beams strengthened with the CFRP anchorage system showed energy absorption indexes reduced by 51.2%-60.6% of their counterparts without the strengthened method. It is evident that the application of the CFRP anchorage system did not enhance the ductility ability but rather reduced it.

Beam CS-5-HL increased its ductility index and energy absorption index by 3.2% and 7.0%, respectively, with respect to beam CS-5-NL. Beam CS-10-HL showed an increase of 3.6% and 7.7% of ductility index and energy absorption index, respectively, in comparison to beam CS-10-NL. Nevertheless, for the beams with severe corrosion damage, due to the early failure of the CFRP anchorage system, the ductility index and energy absorption index of beams CS-20-HL were inferior to beam CS-20-NL. The variation range of these two loads was about 3.2–7.7% of ductility index and energy absorption index of CFRP-strengthened beams except beams with theoretical mass loss of 20%. This further demonstrated that sustained loading has a relatively slight impact on ductility capacity under moderate corrosion conditions, significantly impacting severe corrosion conditions.

3.2.5. *Strain response*

Fig. 15 shows the load-concrete strain curves of the virgin beam (UU) and unstrengthened beams (CU-5-HL, CU-10-HL, CU-20-HL). Similar to the load–deflection curves, these load–strain curves show a similar three-stage response, with three sections and two turning points (corresponding to the cracking of concrete and the yielding of tensile steel). In the first stage (before the generation of the initial crack), the concrete strain increased linearly as the load increased. Prior to the steel bar yielding, the change rate of concrete compressive strain slowed as the corrosion degree increases, and the bearing capacity at the inflection point decreased as well. It served to show that the corrosion obviously reduces the strain rate of concrete in the elastic stage of unstrengthened beams. Following the yielding of the steel bar, the unstrengthened beams responded almost plastically until failure by concrete crushing occurred. No significant correlation was found between the degree of corrosion and the rate of change of concrete compressive strain.

Fig. 16 shows the load-concrete strain relationship of CFRP-strengthened RC beams with different degrees of corrosion. These load–strain curves are found to be virtually identical up to the yield point. This suggested that the trend of concrete strain was not obviously

affected by the corrosion damaged at this stage, which is mainly related to the CFRP anchorage system. After yielding, the concrete strains and fabric strains increased with load in different growth rates depending on the corrosion damage. Beam CS-20-HL showed the highest rate of increase in concrete strains and CFRP strains when compared to the other corroded-strengthen beams.

Fig. 17 shows the outer fabric tensile strains distributions on CFRP sheet along the bond length at different loads for beams CS-5-HL, CS-10-HL, CS-20-HL. The horizontal coordinate represents the distance between the strain gauge and the mid-span, while the vertical coordinate represents the strain value. In the initial stage, the strains of beams strengthened with the CFRP anchorage system was essentially the same as those in the unreinforced beams before concrete cracking. Only the first and second strain gauges near the mid-span generated strain values. Also, the first strain gauge, which was closest to the mid-span, had a substantially higher value than the second strain gauge. Then the concrete began to crack when the tensile strain of concrete in the tensile zone exceeded the ultimate tensile strain. The tension at the crack was shared between the tensioned reinforcement and the CFRP fabric, leading to an increase in the strain growth rate. After yielding of the reinforcement, its stress stayed increased at a low rate and the strain of the CFRP sheet continued to increase at a high rate due to the fact that the additional tension applied to it during fracture was mainly carried by the CFRP anchorage system. With the external load further increasing, interfacial debonding occurred near the mid-span as the tensile stress in the interface approached the interfacial strength. Interfacial stresses were redistributed, and the distal strain reached a maximum, followed by the CFRP anchorage system breaking down.

4. Conclusions

In this paper, an experimental study of the corrosion and flexural behavior of CFRP-strengthened beams under sustained loading and accelerated corrosion has been reported. Based on the experimental results and discussion, the following conclusions can be drawn:

(1) Corroded beams with sustained loading exhibited a higher corrosion level and the maximum corrosion crack width than corroded beams in normal conditions. The external load action led to the microcracks growth, which allowed more chloride ions and oxygen to enter the beam and spread to the surface of the reinforcement, thereby accelerating the process of corrosion of the reinforcement.
(2) Three typical failure modes of the CFRP-strengthened beams were observed: concrete cover separation, debonding of CFRP sheet followed by pulling out of anchors, and matrix cracking and fabric rupture. Beams that failed in the debonding of the CFRP sheet followed by pulling out anchors showed a more ductile behavior.
(3) The unstrengthened beam's ultimate load and yield load decreased with the increase of the corrosion degree of steel bars, but the ductility of concrete beams increased. The use of CFRP anchorage systems enhanced the flexural behavior of the corrosion-damaged beams. Furthermore, CFRP-strengthened beams had a yield load of 95.8 kN to 107 kN, which is well below the control.
(4) The combined corrosion and sustained loading exerted an adverse effect on the load-bearing capacity of the CFRP strengthened RC beams. The yield and ultimate load of the CFRP-strengthened beams with sustained loading were inferior to those without sustained load. And sustained loading had a relatively slight impact on ductility capacity under moderate corrosion conditions, a significant impact at severe corrosion conditions.

CRediT authorship contribution statement

Tanbo Pan: Conceptualization, Methodology, Investigation, Writing – original draft. **Yonglai Zheng:** Supervision, Funding acquisition. **Yujue Zhou:** Conceptualization, Investigation, Writing – review & editing. **Yongcheng Liu:** Methodology, Investigation. **Kunlong Yu:** Investigation. **Yubao Zhou:** Resources.

Declaration of Competing Interest

The authors declare that they have no known competing financial interests or personal relationships that could have appeared to influence the work reported in this paper.

Acknowledgments

The authors are grateful for the financial support from Shanghai International Port (Group) Co. LTD, Department of Education of Fujian Province and Provincial Key Laboratory of Construction Materials & Structural Reinforcement, Sanming University, Sanming, China.

References

[1] Broomfield J. Corrosion of steel in concrete: understanding, investigation and repair. CRC Press; 2003.
[2] Ahmad S. Reinforcement corrosion in concrete structures, its monitoring and service life prediction—a review. Cem Concr Compos 2003;25(4-5):459–71.
[3] Bertolini L, Elsener B, Pedeferri P, Redaelli E, Polder RB. Corrosion of steel in concrete: prevention, diagnosis, repair: John Wiley & Sons, 2013.
[4] Poursaee A. Corrosion of steel in concrete structures. Corrosion of steel in concrete structures. Elsevier 2016:19–33.
[5] François R, Laurens S, Deby F. Corrosion and its consequences for reinforced concrete structures. Elsevier 2018.
[6] Polder RB, Peelen WHA, Courage WMG. Non-traditional assessment and maintenance methods for aging concrete structures–technical and non-technical issues. Mater Corros 2012;63(12):1147–53.
[7] Angst UM. Challenges and opportunities in corrosion of steel in concrete. Mater Struct 2018;51:1–20.
[8] Chen JF, Teng JG. Shear capacity of FRP-strengthened RC beams: FRP debonding. Constr Build Mater 2003;17(1):27–41.
[9] Hollaway LC. Strengthening and rehabilitation of civil infrastructures using fibre-reinforced polymer (FRP) composites: Elsevier, 2008.
[10] Wu H-C, Eamon CD. Strengthening of concrete structures using fiber reinforced polymers (FRP): design, construction and practical applications. 2017.
[11] Kotynia R. FRP Composites for Flexural Strengthening of Concrete Structures: Theory, Testing. Lodz, Poland: Design. Lodz University of Technology; 2019.
[12] Babatunde SA. Review of strengthening techniques for masonry using fiber reinforced polymers. Compos Struct 2017;161:246–55.
[13] Zinno A, Lignola GP, Prota A, Manfredi G, Cosenza E. Influence of free edge stress concentration on effectiveness of FRP confinement. Compos B Eng 2010;41(7):523–32.
[14] Balsamo A, Colombo A, Manfredi G, Negro P, Prota A. Seismic behavior of a full-scale RC frame repaired using CFRP laminates. Eng Struct 2005;27(5):769–80.
[15] Rasheed HA. Strengthening design of reinforced concrete with FRP. CRC Press; 2014.
[16] Sun W, Jirsa JO, Ghannoum WM. Behavior of Anchored Carbon Fiber-Reinforced Polymer Strips Used for Strengthening Concrete Structures. ACI Mater J 2016;113.
[17] Kalfat R, Al-Mahaidi R. Improvement of FRP-to-concrete bond performance using bidirectional fiber patch anchors combined with FRP spike anchors. Compos Struct 2016;155:89–98.
[18] Orton SL, Jirsa JO, Bayrak O. Design considerations of carbon fiber anchors. J Compos Constr 2008;12(6):608–16.
[19] Kalfat R, Al-Mahaidi R, Smith ST. Anchorage devices used to improve the performance of reinforced concrete beams retrofitted with FRP composites: State-of-the-art review. J Compos Constr 2013;17(1):14–33.
[20] del Rey Castillo E, Kanitkar R, Smith ST, Griffith MC, Ingham JM. Design approach for FRP spike anchors in FRP-strengthened RC structures. Compos Struct 2019;214:23–33.
[21] Zheng Y, Zhou Y, Zhou Y, Pan T, Zhang Q, Liu D. Cracking behavior of reinforced concrete beams strengthened with CFRP anchorage system under cyclic and monotonic loading. Eng Struct 2020;207:110222. https://doi.org/10.1016/j.engstruct.2020.110222.
[22] Kim Y, Quinn K, Ghannoum WM, Jirsa JO. Strengthening of Reinforced Concrete T-Beams Using Anchored CFRP Materials. ACI Struct J 2014;111.
[23] Koutas L, Triantafillou TC. Use of anchors in shear strengthening of reinforced concrete T-beams with FRP. J Compos Constr 2013;17(1):101–7.
[24] Zaki MA, Rasheed HA, Roukerd RR, Raheem M. Performance of reinforced concrete T beams strengthened with flexural CFRP sheets and secured using CFRP

splay anchors. Eng Struct 2020;210:110304. https://doi.org/10.1016/j.engstruct.2020.110304.
[25] El Maaddawy T, Soudki K, Topper T. Performance evaluation of carbon fiber-reinforced polymer-repaired beams under corrosive environmental conditions. ACI Struct J 2007;104:3.
[26] Zhou Y, Dang L, Sui L, Li D, Zhao X, Xing F, et al. Experimental study on the bond behavior between corroded rebar and concrete under dual action of FRP confinement and sustained loading. Constr Build Mater 2017;155:605–16.
[27] Abouhussien AA, Hassan AAA. Acoustic emission monitoring of corrosion damage propagation in large-scale reinforced concrete beams. J Perform Constr Facil 2018;32(2):04017133. https://doi.org/10.1061/(ASCE)CF.1943-5509.0001127.
[28] El Maaddawy TA, Soudki KA. Effectiveness of impressed current technique to simulate corrosion of steel reinforcement in concrete. J Mater Civ Eng 2003;15(1):41–7.
[29] Smith ST, Hu S, Kim SJ, Seracino R. FRP-strengthened RC slabs anchored with FRP anchors. Eng Struct 2011;33(4):1075–87.
[30] Zhang HW, Smith ST. Influence of FRP anchor fan configuration and dowel angle on anchoring FRP plates. Compos B Eng 2012;43(8):3516–27.
[31] Llauradó PV, Fernández-Gómez J, González Ramos FJ. Influence of geometrical and installation parameters on performance of CFRP anchors. Compos Struct 2017;176:105–16.
[32] Zhang HW, Smith ST, Kim SJ. Optimisation of carbon and glass FRP anchor design. Constr Build Mater 2012;32:1–12.
[33] Metals ACG-oCo. Standard practice for preparing, cleaning, and evaluating corrosion test specimens: ASTM international, 2017.
[34] Hime W, Backus L, Li C. Modeling time-to-corrosion cracking in chloride contaminated reinforced concrete structures. Discussions and closure. Aci Mater J 1999;96.
[35] Smith ST, Teng JG. Shear-bending interaction in debonding failures of FRP-plated RC beams. Adv Struct Eng 2003;6(3):183–99.
[36] You Y-C, Choi K-S, Kim J. An experimental investigation on flexural behavior of RC beams strengthened with prestressed CFRP strips using a durable anchorage system. Compos B Eng 2012;43(8):3026–36.
[37] Elghazy M, El Refai A, Ebead U, Nanni A. Post-repair flexural performance of corrosion-damaged beams rehabilitated with fabric-reinforced cementitious matrix (FRCM). Constr Build Mater 2018;166:732–44.